Electronic supplementary information

All-wood, Low Tortuosity, Aqueous, Biodegradable Supercapacitors with Ultra-High Capacitance

Chaoji Chen[1,2,†], Ying Zhang[2,†], Yiju Li[2], Jiaqi Dai[2], Jianwei Song[2], Yonggang Yao[2], Yunhui Gong[2], Iain Kierzewski[2], Jia Xie[1,*], Liangbing Hu[2,*]

Method S1: Calculation details

a. **Single Electrode in the three-electrode cell configuration**

The areal and specific capacitances of the electrodes are all calculated from their GCD profiles by the following equations:

$$C_{(areal)} = \frac{I * \Delta t}{S * \Delta V}$$

$$C_{(specific)} = \frac{I * \Delta t}{m * \Delta V}$$

where I is the discharge current, Δt is the discharge time, S is the effective area of the electrode, ΔV is the potential window of the discharge process, and m is the mass of the electrode.

b. **All-wood-structured ASC Device**

The areal and specific capacitances of the ASC device are calculated from the GCD profiles according to the following equation:

$$C_{(areal)} = \frac{I * \Delta t}{S * \Delta V}$$

—

where I is the discharge current, Δt is the discharge time, S is the area of the electrode, ΔV is the voltage difference from the beginning to the end of an individual discharge cycle and m is the total mass of the negative and positive electrode materials.

Calculation details of the energy (E) and power densities (P):

$$E = 0.5*C*\Delta V^2$$

$$P = E/\Delta t$$

where C is the areal or specific capacitance of the ASC device, Δt and ΔV are the discharge time and potential difference of an individual discharge cycle.

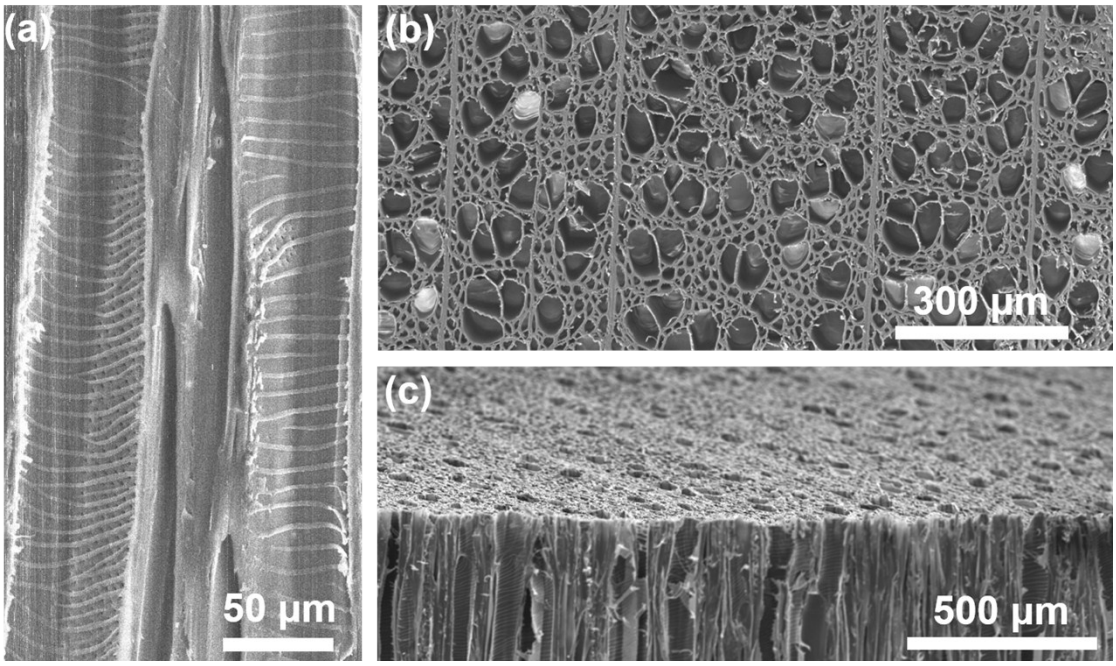

Figure S1. SEM images of the nature wood: (a) cross-section-view image showing the channels, (b) top-view image, (c) cross-section-view image showing both the top and cross section of the nature wood.

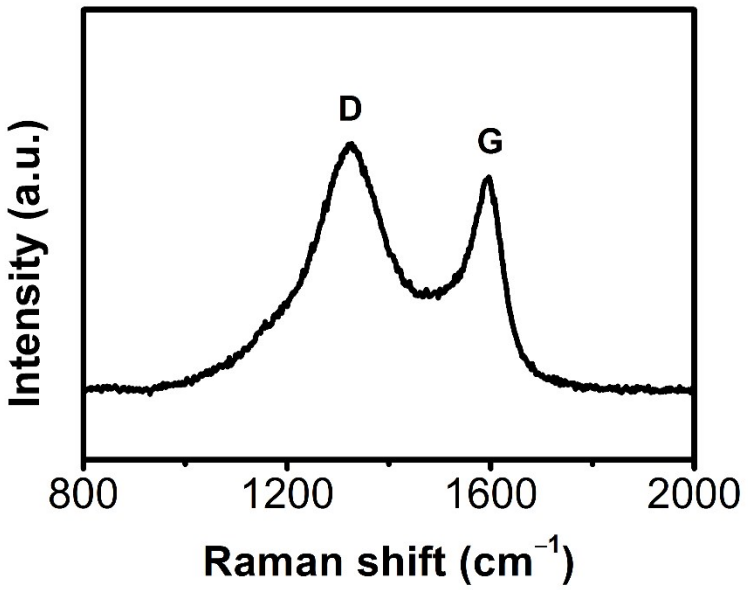

Figure S2. Raman spectrum of the activated wood carbon. The intensity ratio of the D and G peaks (I_D/I_G) is 1.1.

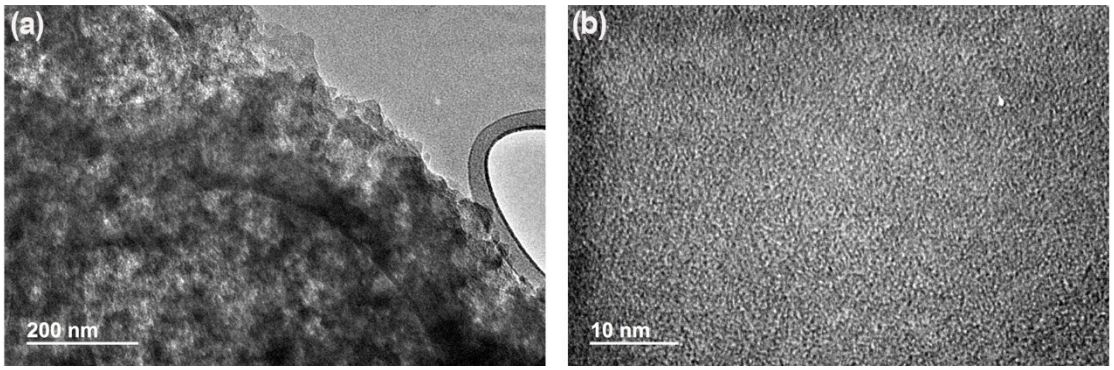

Figure S3. TEM images of the activated wood carbon.

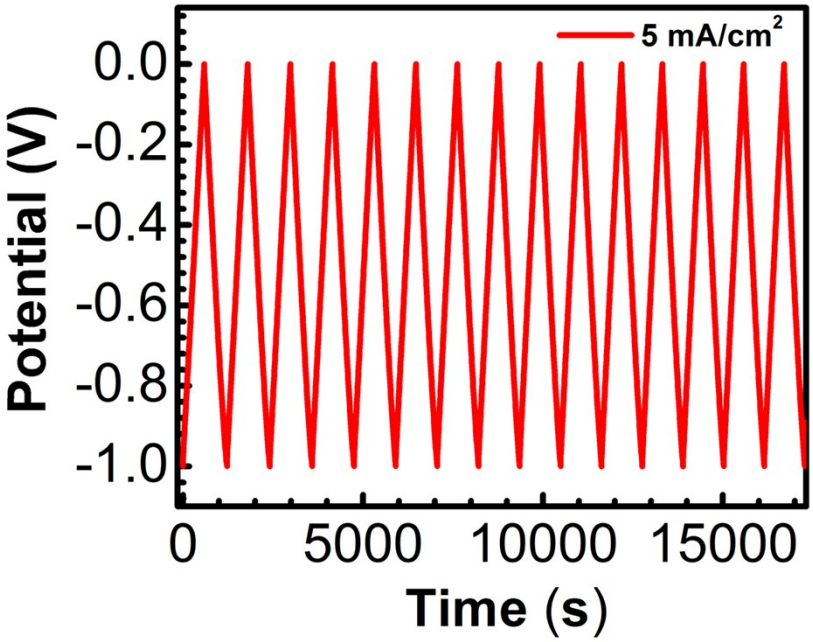

Figure S4. Charge-discharge profiles of the AWC anode of the initial 15 cycles at 5 mA cm^{-2}.

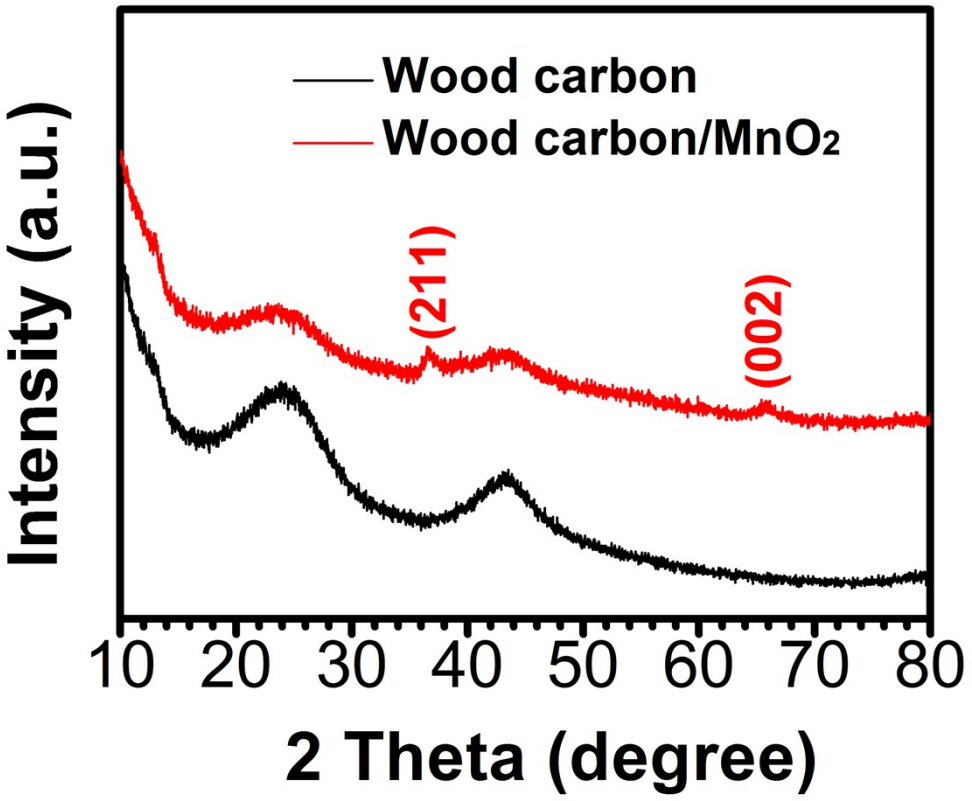

Figure S5. XRD patterns of the wood carbon and MnO_2/wood carbon composite.

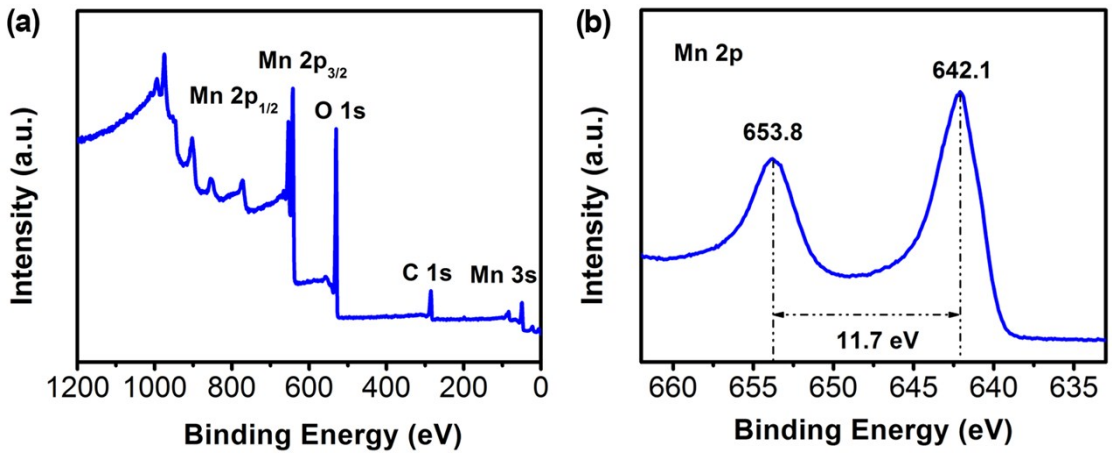

Figure S6. XPS spectra for the MnO_2/WC composite: (a) survey XPS and (b) high-resolution Mn 2p spectra. As reported, the Mn oxidation state can be determined by the binding energy width (ΔE) between the separated Mn 2p peaks caused by multiplet splitting.[1] The Δ*E* data of 11.7 eV for the Mn 2p indicates that the as-grown manganese oxide is MnO_2.

Ref [1]. Z. Fan, J. Yan, T. Wei, L. Zhi, G. Ning, T. Li, F. Wei, *Advanced Functional Materials* 2011, *21*, 2366-2375.

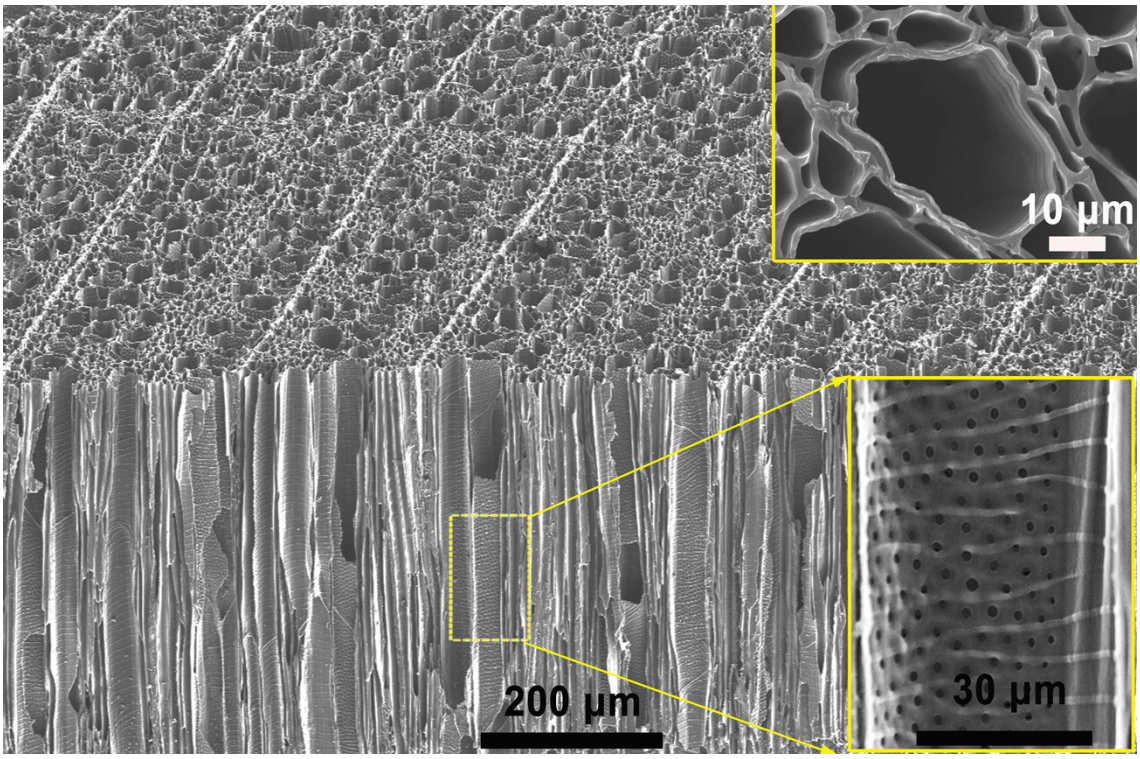

Figure S7. SEM images of the wood carbon.

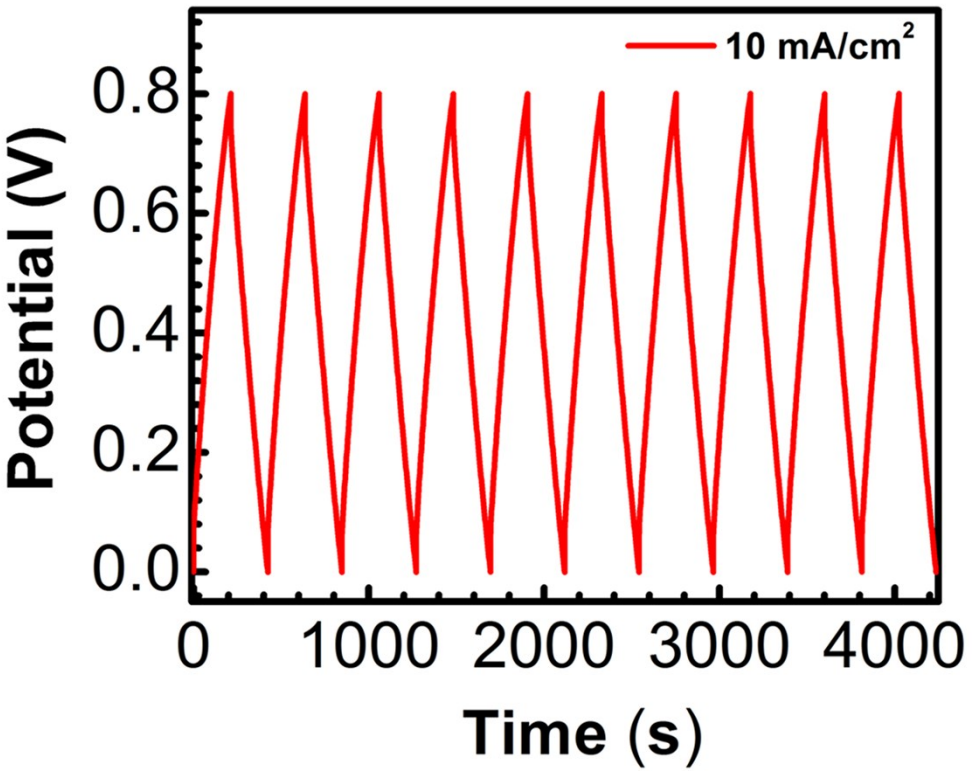

Figure S8. The charge-discharge profiles of the MnO_2@WC cathode at 10 mA cm^{-2} in the initial 10 cycles.

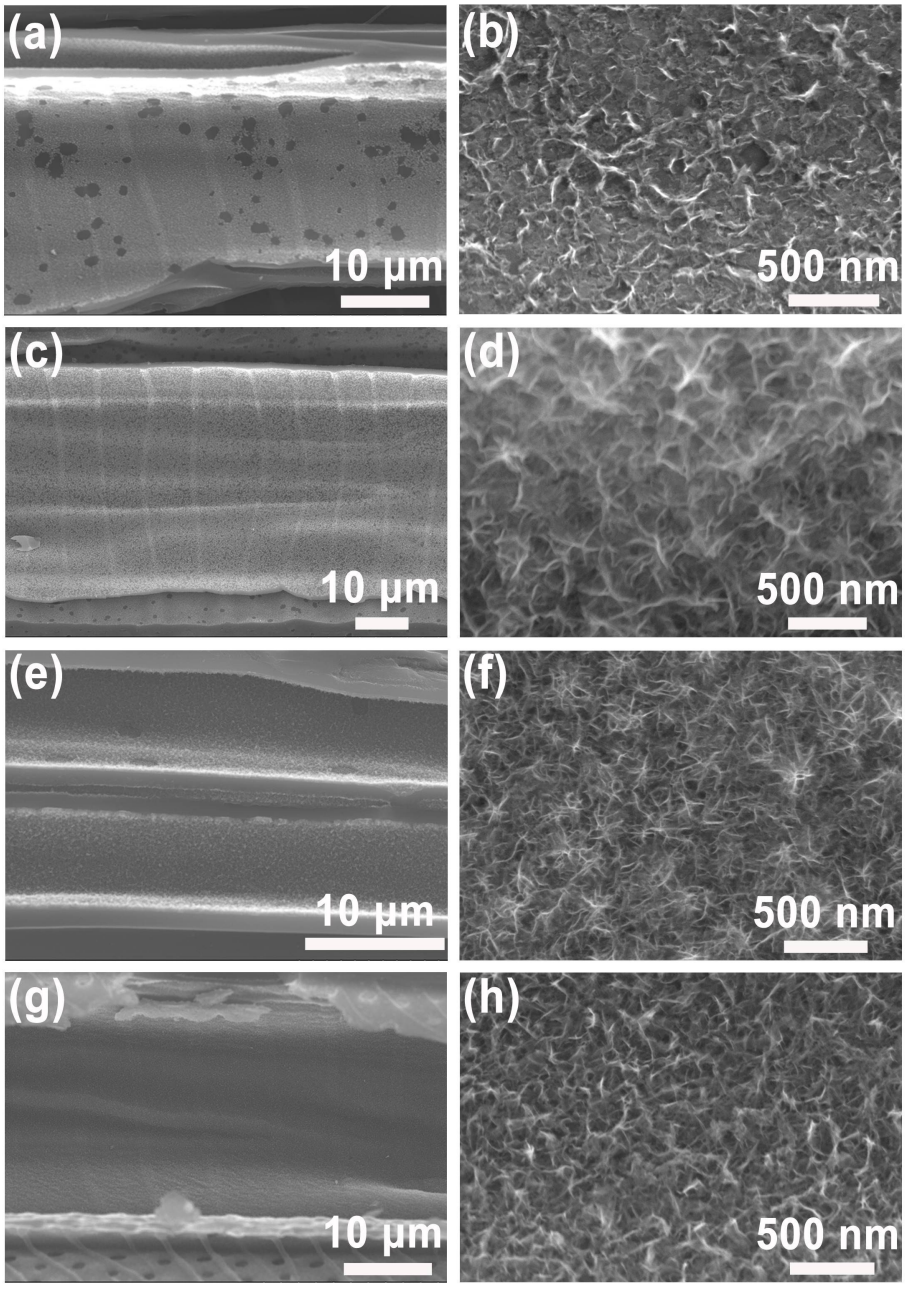

Figure S9. SEM images of the WC-MnO_2 products obtained with different electrodeposition times: (a,b) 1h, (c,d) 2h, (e,f) 5 h and (g,h) 10 h.

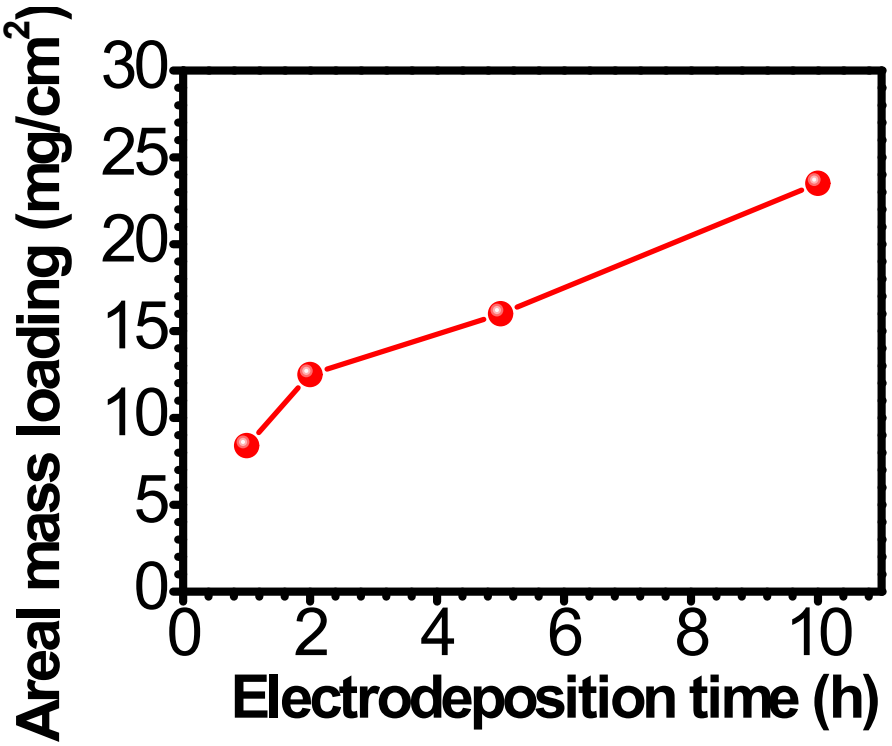

Figure S10. Areal mass loadings of MnO_2 in the wood carbon/MnO_2 products obtained with different electrodeposition times.

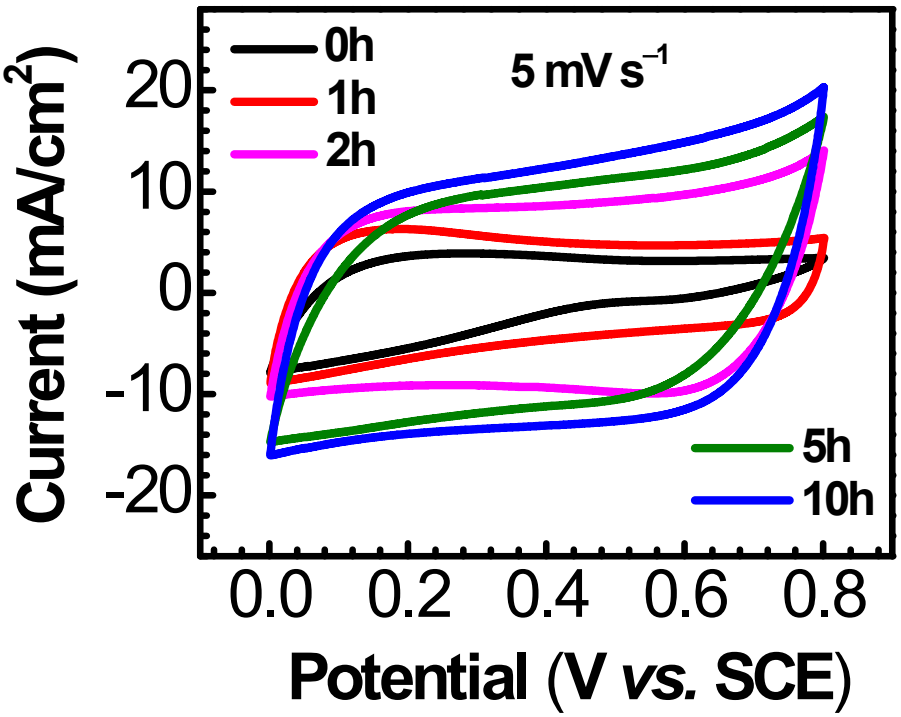

Figure S11. CV curves of the WC-MnO_2 products obtained with different electrodeposition times at a scan rate of 5 mV s^{-1}.

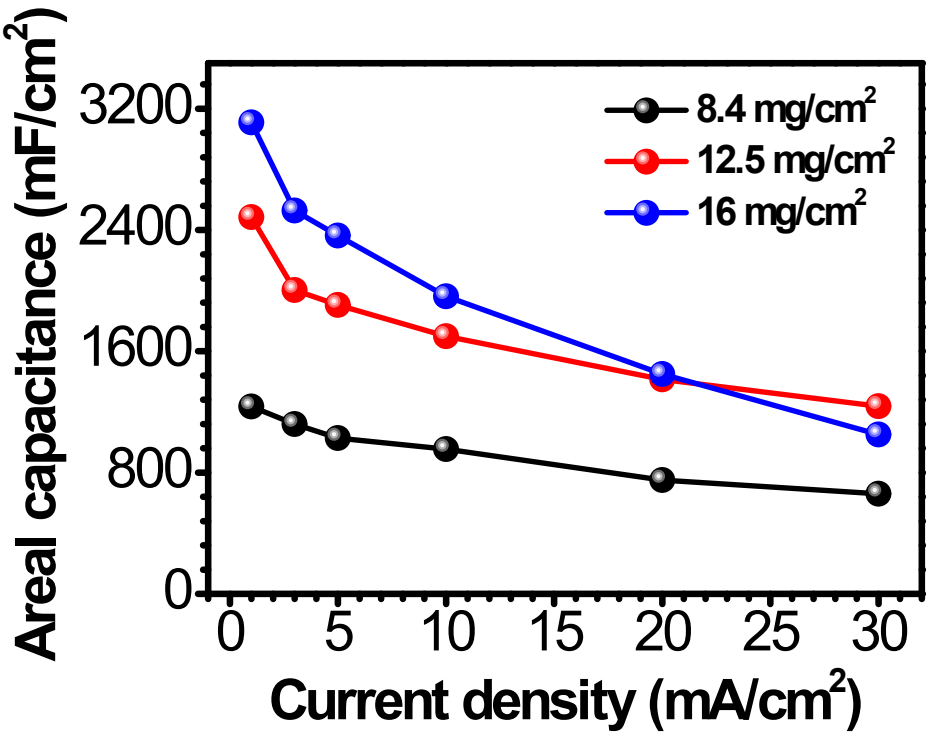

Figure S12. Rate performances of the MnO_2/wood carbon electrodes with different areal mass loadings of MnO_2 (1h: 8.4 mg/cm^2, 2h: 12.5 mg/cm^2, 5h: 16 mg/cm^2).

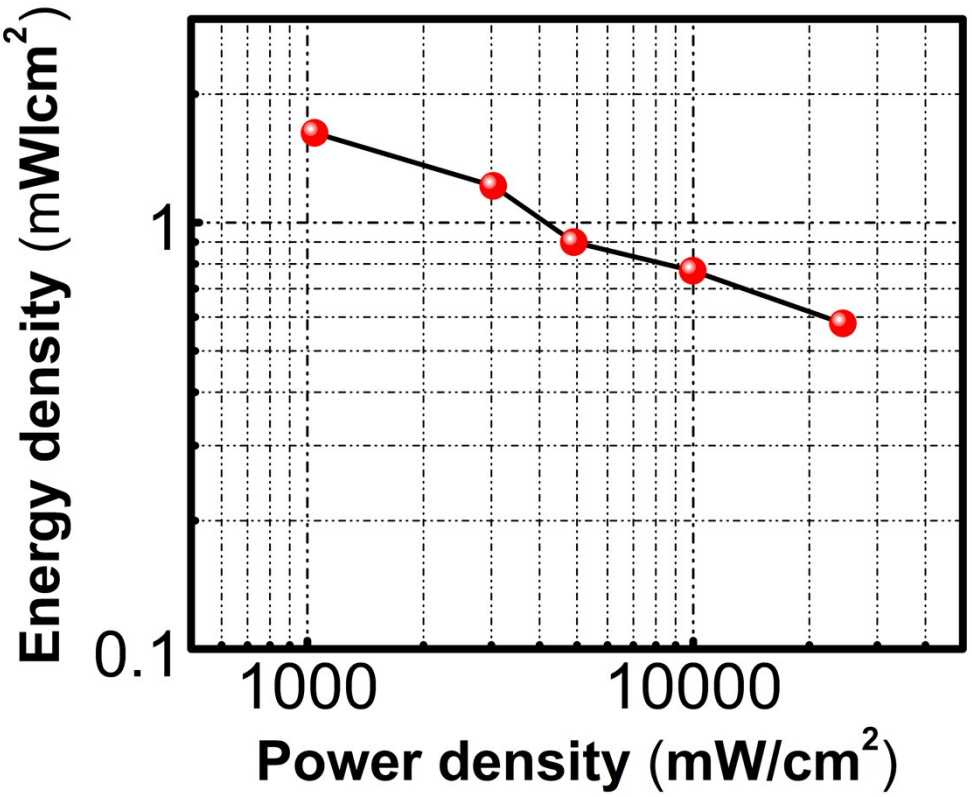

Figure S13. Areal energy and power densities of the ACS device, including masses of all components.

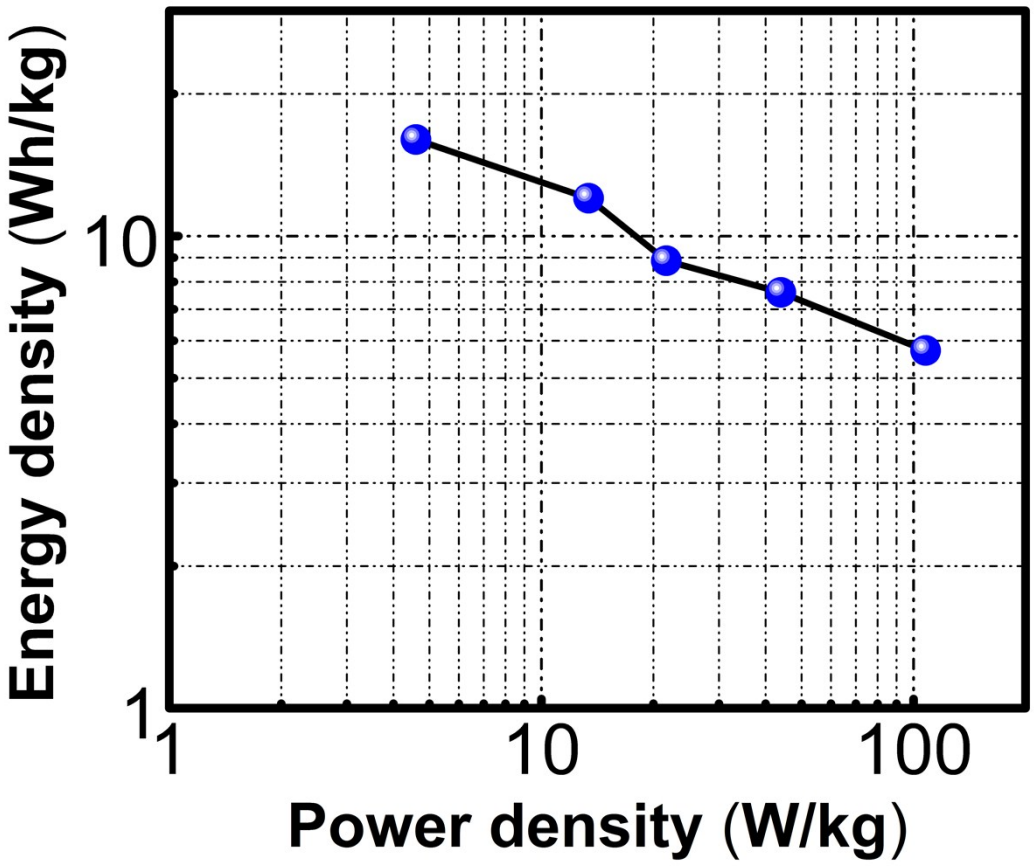

Figure S14. Specific energy and power densities of the ACS device calculated based on the total mass of the activated wood carbon anode, MnO_2@WC cathode electrode materials and wood membrane separator.

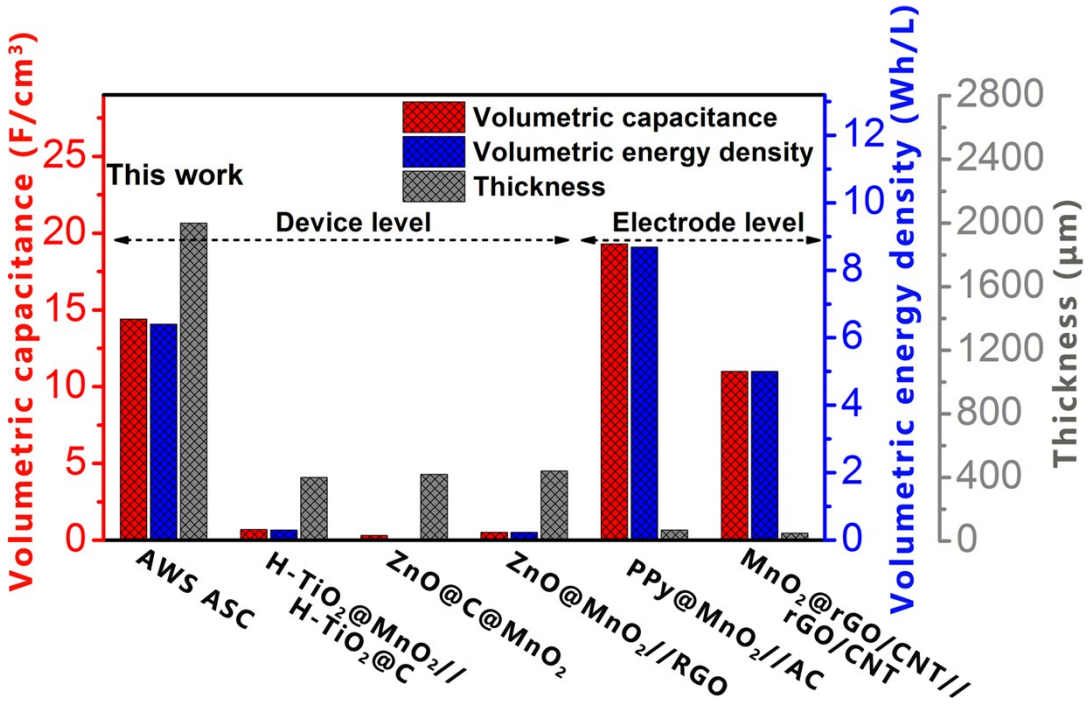

Figure S15. Volumetric capacitance, energy density and thickness of the all-wood-structured ASC (AWS ASC) compared with the previous reported electrode materials (H-TiO_2@MnO_2//H-TiO_2@C[14], ZnO@C@MnO_2[7], ZnO@MnO_2//RGO[2], PPy@MnO_2//AC[11] and MnO_2@rGO/CNT//rGO/CNT[12]).

Table S1: Volumetric capacitance and energy density comparison of MnO_2-based and some carbon-/metal oxide/nitrite-based supercapacitors.

Material name	Volumetric capacitance	Volumetric energy density	Cycling stability	Calculation method	Sources
WO_{3-x}/MoO_{3-x}//PANI/carbon	0.216 F/cm^3	1.9 Wh/L	10000	Electrode level	Ref. [1]
ZnO@MnO_2//RGO	0.52 F/cm^3	0.234 Wh/L	5000	Device level	Ref. [2]
Co_9S_8//Co_3O_4@RuO_2	4.28 F/cm^3	1.21 Wh/L	2000	Device level	Ref. [3]
VO_x//VN	1.35 F/cm^3	0.61 Wh/L	-	Device level	Ref. [4]
TiN	0.33 F/cm^3	0.05 Wh/L	15000	Device level	Ref. [5]
TiO_2@C	0.125 F/cm^3	0.011 Wh/L	5000	Device level	Ref. [6]
ZnO@C@MnO_2	0.325 F/cm^3	0.04 Wh/L	10000	Device level	Ref. [7]
VN/CNT	7.9 F/cm3	0.54 Wh/L	10000	Device level	Ref. [8]

Carbon Nanotube Fiber	13.5 F/cm3	1.32 Wh/L	10000	Electrode level	Ref. [9]
Mesoporous carbon	17.4 F/cm3	6.2 Wh/L	5000	Electrode level	Ref. [10]
Polypyrrole@MnO_2//AC	19.3 F/cm3	8.69 Wh/L	1000	Electrode level	Ref. [11]
MnO_2-coated rGO/SWCNT//rGO/SWCNT	11 F/cm3	5 Wh/L	10000	Electrode level	Ref. [12]
Carbon/MnO_2 fiber	2.5 F/cm3	0.12 Wh/L	10000	Device level	Ref. [13]
H-TiO_2@MnO_2//H-TiO_2@C	0.7 F/cm3	0.3 Wh/L	5000	Device level	Ref. [14]
Bamboo-like carbon	2.1 F/cm3	0.24 Wh/L	5000	Device level	Ref. [15]
All-wood-structured ASC	**14.4 F/cm3**	**6.4 Wh/L**	**10000**	**Device level**	**This work**

Refs:

[1] X. Xiao, T. Ding, L. Yuan, Y. Shen, Q. Zhong, X. Zhang, Y. Cao, B. Hu, T. Zhai, L. Gong, J. Chen, Y. Tong, J. Zhou and Z. L. Wang, *Adv. Energy Mater.*, 2012, **2**, 1328

[2] W. Zilong, Z. Zhu, J. Qiu and S. Yang, *J. Mater. Chem. C*, 2014, **2**, 1331

[3] J. Xu, Q. Wang, X. Wang, Q. Xiang, B. Liang, D. Chen and G. Shen, *ACS Nano*, 2013, **7**, 5453

[4] X. Lu, M.-H. Yu, T. Zhai, G. Wang, S. Xie, T. Lu, C. Liang, Y.-X. Tong and Y. Li, *Nano Lett.*, 2013, 2628

[5] X. H. Lu, G. M. Wang, T. Zhai, M. H. Yu, S. L. Xie, Y. C. Ling, C. L. Liang, Y. X. Tong and Y. Li, *Nano Lett.*, 2012, **12**, 5376

[6] H. Zheng, T. Zhai, M. Yu, S. Xie, C. Liang, W. Zhao, S. C. I. Wang, Z. Zhang and X. Lu, *J. Mater. Chem. C*, 2013, **1**, 225

[7] P. Yang, X. Xiao, Y. Li, Y. Ding, P. Qiang, X. Tan, W. Mai, Z. Lin, W. Wu, T. Li, H. Jin, P. Liu, J. Zhou, C. P. Wong and Z. L. Wang, *ACS Nano*, 2013, **7**, 2617

[8] X. Xiao, X. Peng, H. Jin, T. Li, C. Zhang, B. Gao, B. Hu, K. Huo and J. Zhou, *Adv. Mater.*, 2013, **25**, 5091

[9] Xu P, Gu T, Cao Z, et al. Adv. Energy Mater. 2014, **4**, 1300759

[10] Wang Q, Yan J, Wei T, et al. Carbon, 2013, **60**, 481-487

[11] Tao J, Liu N, Li L, et al. Nanoscale, 2014, **6**, 2922-2928

[12] Yu, D., Goh, K., Zhang, Q., Wei, L., Wang, H., Jiang, W. and Chen, Y. Adv. Mater., 2014, **26**, 6790–6797

[13] X. Xiao, T. Li, P. Yang, Y. Gao, H. Jin, W. Ni, W. Zhan, X. Zhang, Y. Cao, J. Zhong, L. Gong, W. C. Yen, W. Mai, J. Chen, K. Huo, Y. L. Chueh, Z. L. Wang and J. Zhou, *ACS Nano*, 2012, **6**, 9200

[14] X. Lu, M. Yu, G. Wang, T. Zhai, S. Xie, Y. Ling, Y. Tong and Y. Li, *Adv. Mater.*, 2013, **25**, 267

[15] Sun Y, Sills R B, Hu X, et al. Nano letters, 2015, **15**, 3899-3906.

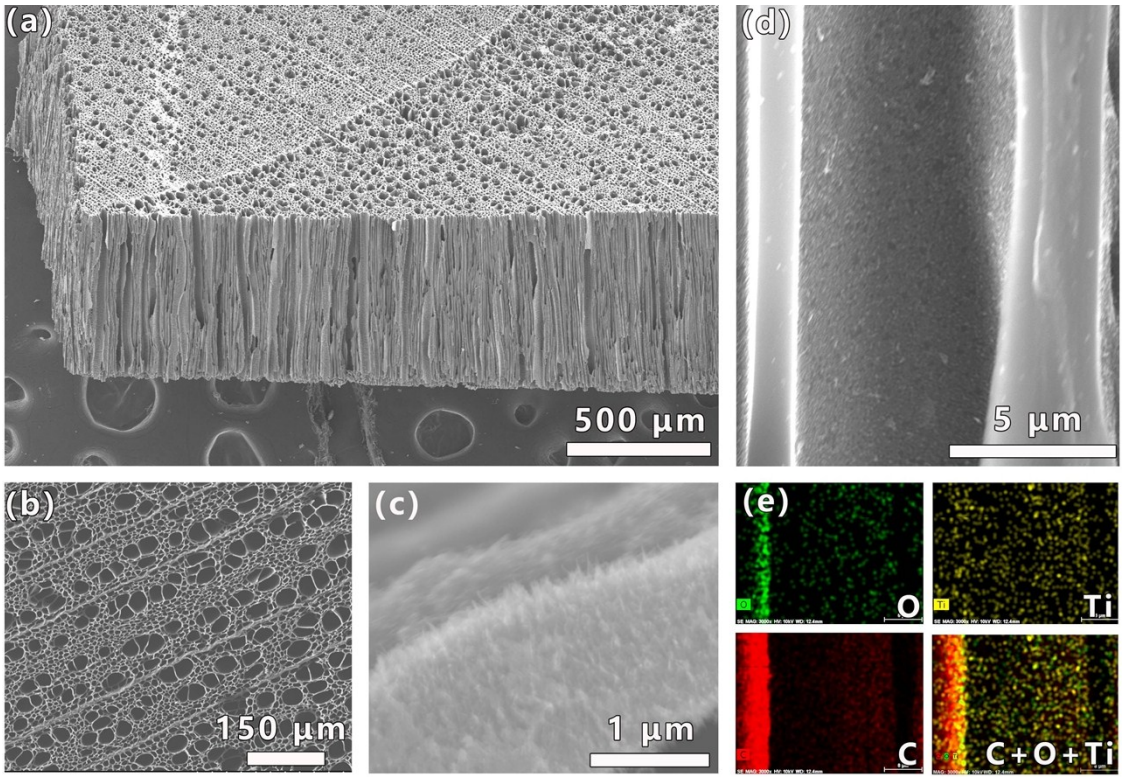

Figure S16. Structure and morphology characterizations of the TiO_2@WC composite. (a) cross-section-view, (b) top-view, (c) magnified top-view and (d) magnified cross-section-view SEM images. (e) Element mapping images of O, Ti, C and their integration.

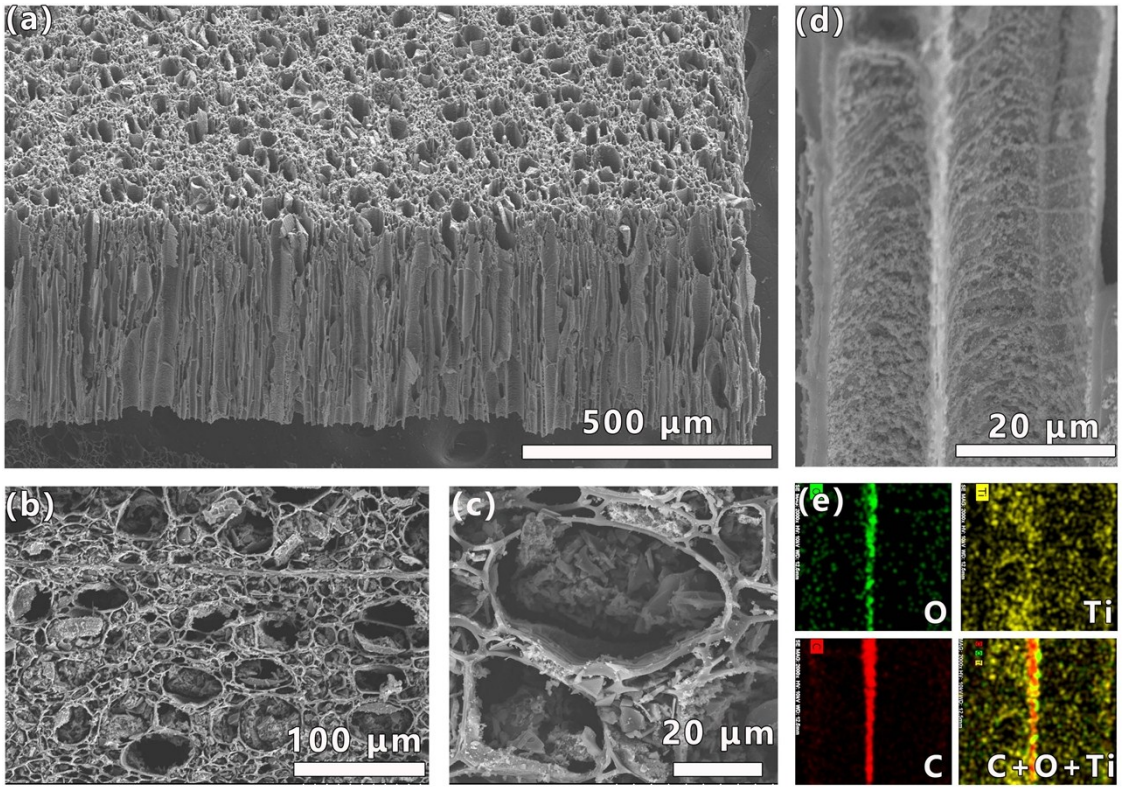

Figure S17. Structure and morphology characterizations of the LTO@WC composite. (a) cross-section-view, (b) top-view, (c) magnified top-view and (d) magnified cross-section-view SEM images. (e) Element mapping images of O, Ti, C and their integration.

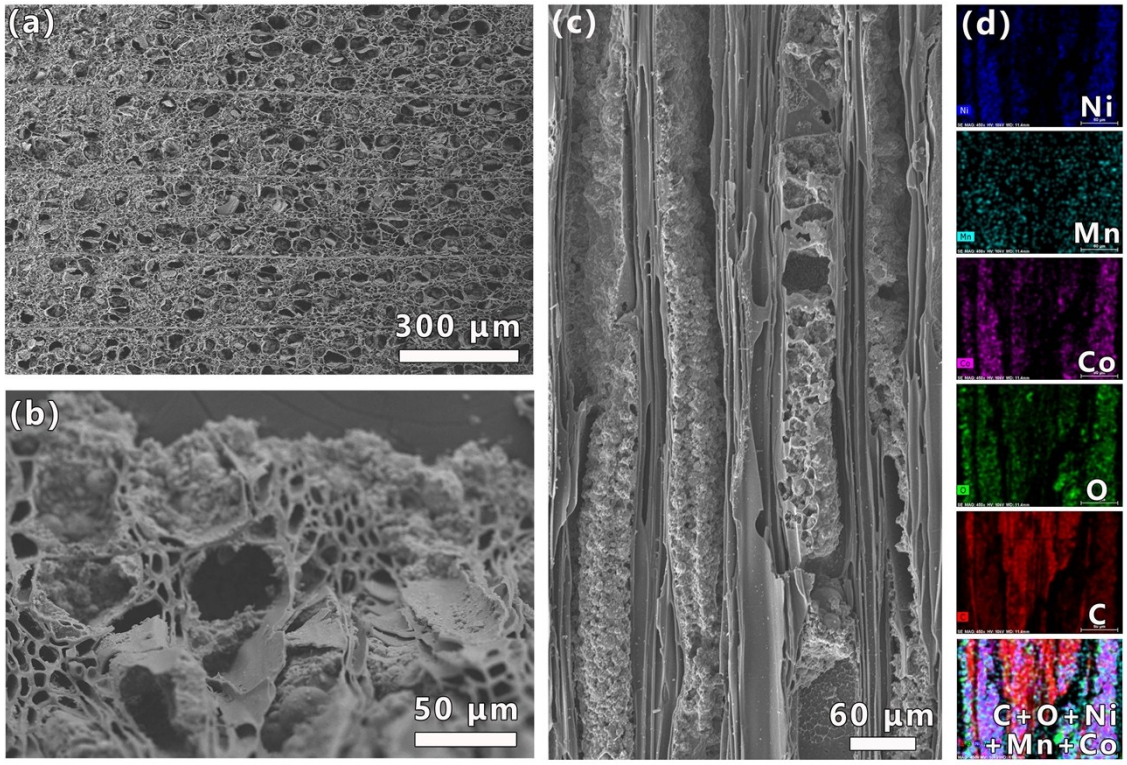

Figure S18. Structure and morphology characterizations of the NMC@WC composite. (a) top-view, (b) magnified top-view and (c) cross-section-view SEM images. (d) Element mapping images of Ni, Mn, Co, O, C and their integration.

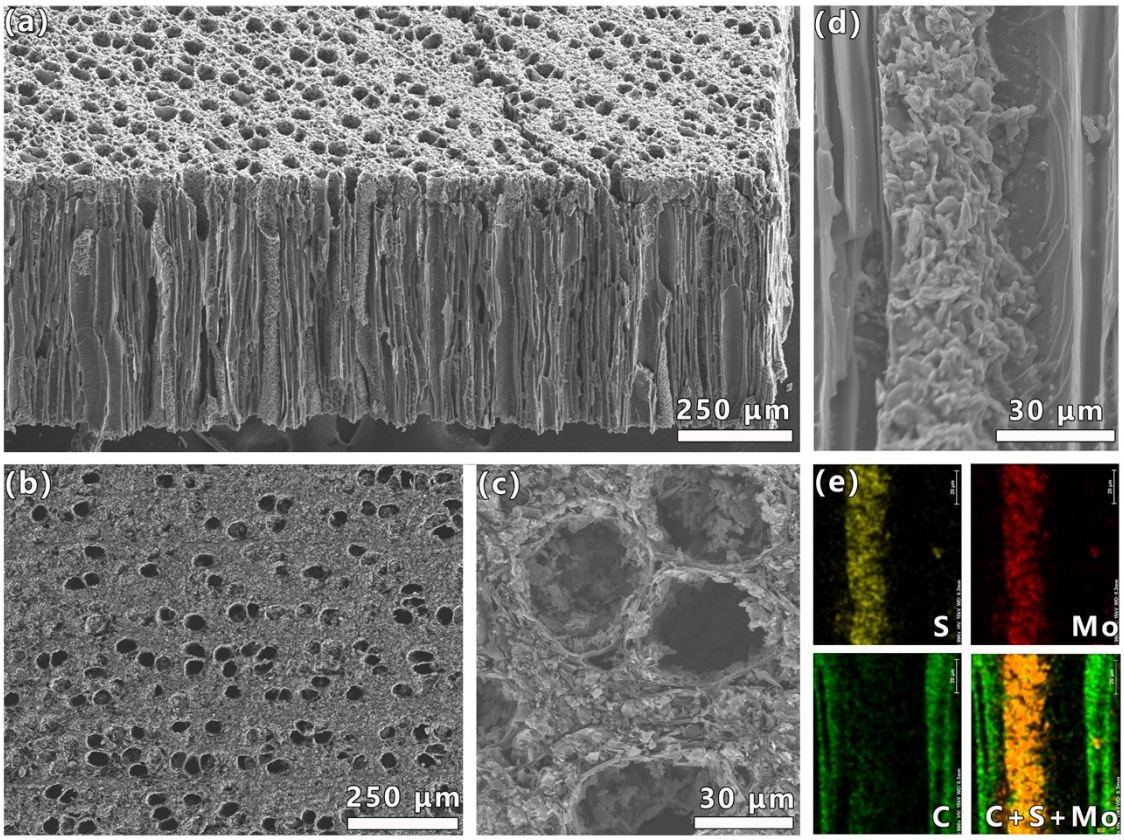

Figure S19. Structure and morphology characterizations of the MoS_2@WC composite. (a) cross-section-view, (b) top-view, (c) magnified top-view and (d) magnified cross-section-view SEM images. (e) Element mapping images of S, Mo, C and their integration.

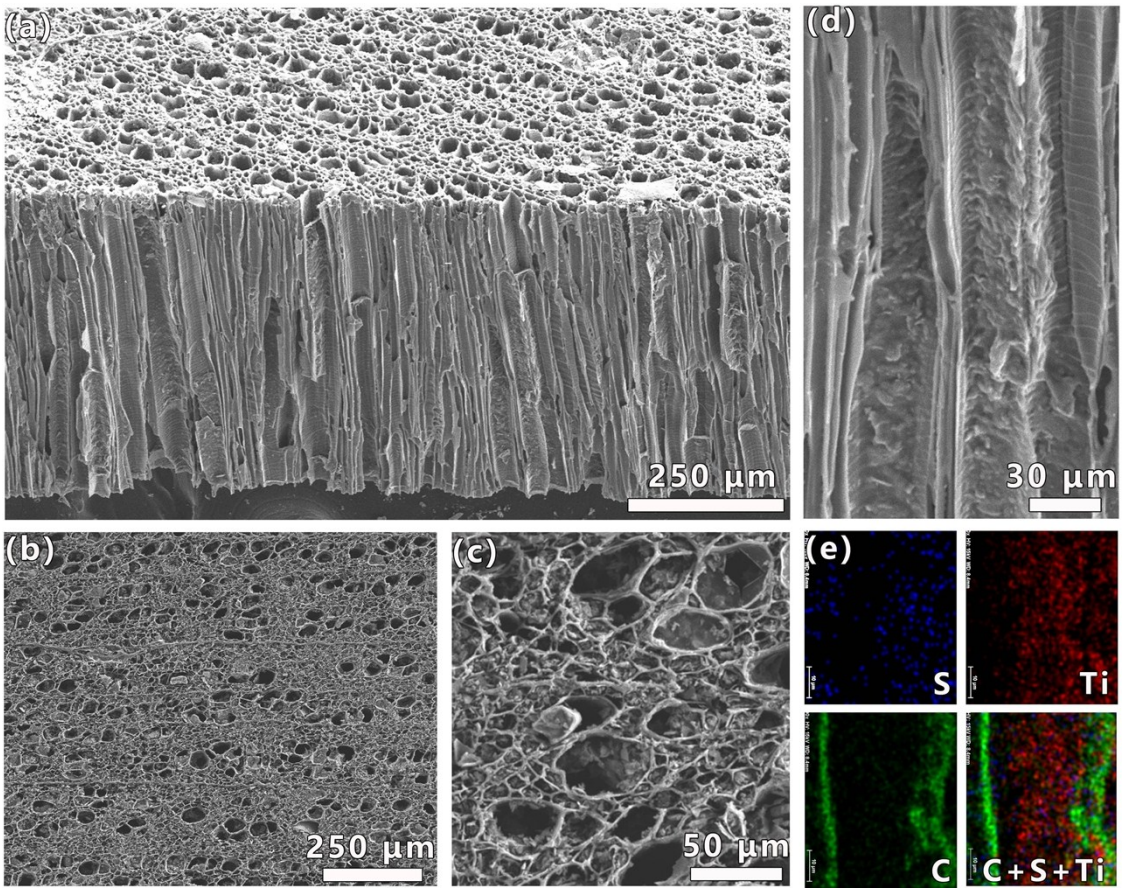

Figure S20. Structure and morphology characterizations of the TiS_2@WC composite. (a) cross-section-view, (b) top-view, (c) magnified top-view and (d) magnified cross-section-view SEM images. (e) Element mapping images of S, Ti, C and their integration.

The universality of our approach lies in these aspects:

- Universal electroactive materials (metal sulfides, oxides and so on);
- Universal synthesis method (electrodeposition, hydrothermal, vacuum-assisted infiltration, *et al.*);
- Universal functions (supercapacitor, rechargeable batteries, electrocatalysis, photocatalysis, *et al.*).

Table S2. Summaries of the universality of the wood-structure-inspired materials design.

Material name	Electroactive material	Synthesis method	Function
MnO_2@WC	MnO_2	Electrodeposition	SCs
TiO_2@WC	TiO_2	Hydrothermal	LIBs/SIBs (anode)/Photocatalysis
LTO@WC	LTO	Vacuum-assisted infiltration	LIBs/SIBs (anode)
NMC@WC	NMC	Vacuum-assisted infiltration	LIBs (cathode)
TiS_2@WC	TiS_2	Vacuum-assisted infiltration	LIBs (anode)/SCs
MoS_2@WC	MoS_2	Vacuum-assisted infiltration	LIBs/SIBs (anode)/SCs/Electrocatalysis